Journal of Structural Geology 31 (2009) 1597–1611

Contents lists available at ScienceDirect

Journal of Structural Geology

journal homepage: www.elsevier.com/locate/jsg

Internal geometry and growth history of a thrust-related anticline in a deep water fold belt

Simon Higgins [a,*,1], Benjamin Clarke [b,2], Richard J. Davies [c], Joe Cartwright [a]

[a] 3DLab, School of Earth, Ocean and Planetary Sciences, Cardiff University, Main Building, Park Place, Cardiff, CF10 3YE, UK
[b] Statoil ASA (Global Exploration), 4035 Stavanger, Norway
[c] CeREES, (Centre for Research into Earth Energy Systems) Department of Earth Sciences, University of Durham, Science Labs, Durham DH1 3LE, UK

ARTICLE INFO

Article history:
Received 19 December 2007
Received in revised form
20 July 2009
Accepted 29 July 2009
Available online 4 August 2009

Keywords:
Fold growth
Fault linkage
Strain distribution
Deep water
Niger Delta

ABSTRACT

Although 3D seismic imaging has become a fundamental tool for the analysis of extensional fault geometries and their development, it has not been utilised to the same degree to investigate the structure and growth history of thrust faults. Here, the structural evolution of a fold and thrust belt is investigated through the analysis of an isolated fold imaged in the deep water Niger Delta. A quantitative description of thrust fault displacement through transfer zones is presented to investigate the internal structure of a complex fault-related fold, while syn-kinematic growth packages are used to chart fold growth through time, so as to also understand the early growth history. Results reveal that a number of initially separate folds coalesced along the axial trends into a single structural culmination. Numerous thrust faults with similar and opposing dip, link and transfer displacement within the structure as it changes vergence along strike. The distribution of bulk deformation along the fault-related fold is simple, systematic and similar to that observed for extensional fault systems. Deficits in fault heave, both in the form of perturbations on non-linking or aggregated profiles, and displacement minima within transfer zones, are compensated to some degree by an increase in fold-related strain. Despite this accommodation, fold amplitude or crest elevation is largely unaffected by variations in fault heave. The observations for this isolated fold should be widely applicable to fold and fault development in more complex areas.

1. Introduction

The relationship between thrust faults and associated folds has been extensively researched in the past two decades. Distinct classes of structure are now clearly defined and widely described from orogenic belts exposed on land and more recently from fold and thrust belts associated with gravity-driven deformation of continental margins. The description of fault-bend folds (Rich, 1934; Boyer and Elliot, 1982; Suppe, 1983), fault-displacement-gradient folds (Williams and Chapman, 1983; Suppe, 1985; Suppe and Medwedeff, 1990; Wickham, 1995), break-thrust folds (Jamison, 1987; Mitchell and Woodward, 1988; Butler, 1992; Woodward, 1992) and detachment folds at the lateral terminations of faults (e.g. Jamison, 1987) have mainly been based on cross-sectional geometry, either derived from exposed sections or from 2D seismic profiles. However, our current understanding of the initiation, propagation and along strike linkage of such structures remains limited, although analogue and numerical models have led to significant advances (e.g. Liu and Dixon, 1991). The advent of 3D seismic data as a research tool has been a major factor in our understanding of normal-fault propagation and linkage (Childs et al., 1995; Nicol et al., 1995, 1996; Meyer et al., 2002). Thus far, this imaging approach has not been employed to the same degree to analyse the three-dimensional evolution of thrust-related folds.

A primary aim of this paper is to demonstrate the potential for the use of 3D seismic data in the structural analysis of fold and thrust belts. Advancements in seismic imaging resulting from modern 3D migration algorithms enable thrusts to be accurately mapped and to reveal geometrical subtleties that are vital for the correct reconstruction of growth histories. We use the example of a superficially simple fold structure from a deepwater fold and thrust belt of the Niger Delta (Corredor et al., 2005; Briggs et al., 2006) to analyse fold and thrust growth histories through detailed strain analysis. We describe several techniques to define the strain history, and we show that a single, kinematically coherent structure evolved by a process of segment linkage directly analogous to that for normal faults (e.g. Segall and Pollard, 1980; Ellis and Dunlap,

* Corresponding author.
E-mail addresses: sihi@statoilhydro.com (S. Higgins), ben.clarke@canamens.com (B. Clarke), richard.davies@durham.ac.uk (R.J. Davies), cartwrightja@cardiff.ac.uk (J. Cartwright).
1 Present address: StatoilHydro ASA, 4035 Stavanger, Norway.
2 Present address: Canamens Energy AS, Postboks 130, 4065 Stavanger, Norway.

0191-8141/$ – see front matter © 2009 Elsevier Ltd. All rights reserved.
doi:10.1016/j.jsg.2009.07.006

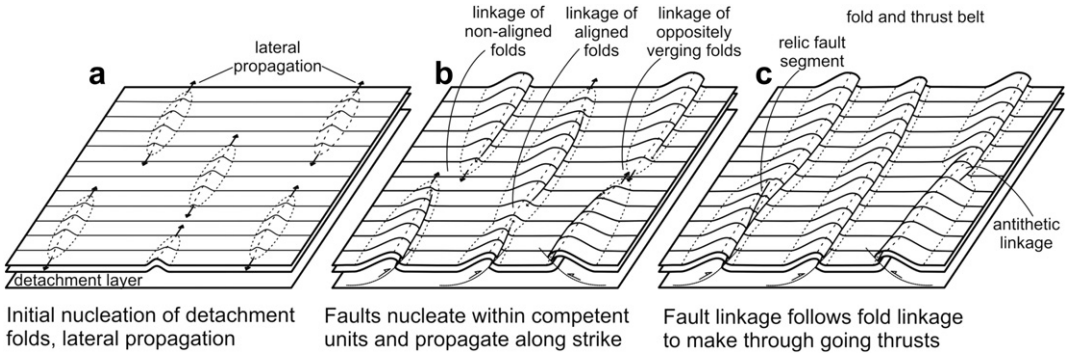

Fig. 1. An example of a model for the structural evolution of a fold and thrust belt, based partly upon and expanded from the modelling results of Liu and Dixon (1991). (a) Numerous low-amplitude detachment folds initiate and grow by lateral propagation. (b) Faults nucleate within competent units and propagate along strike within the folds. Forethrusts form in the forelimbs, backthrusts in the backlimbs. Each fold may nucleate a number of faults along its length. (c) Fault linkage follows fold linkage creating through-going thrust surfaces.

1988; Peacock and Sanderson, 1991; Cartwright et al., 1995). Linkage of propagating segments to form thrust faults with relay structures or transfer zones is not a new concept (Dahlstrom, 1970; Elliot, 1976; Ellis and Dunlap, 1988; Nicol et al., 2002) and some model based studies have postulated that thrust fault linkage follows the along strike propagation and merger of collinear, periclinal detachment folds (e.g. Liu and Dixon, 1991) (Fig. 1). However the use of 3D seismic data to test the observations and constrain the interpretations has not previously been published for fold and thrust settings.

The paper concludes with a discussion of the growth history of a well-constrained fold in the context of current uncertainties about thrust-related fold evolution (e.g., Thorbjornsen and Dunne, 1997), for the purpose of evaluating fault-related fold models. The quantitative description of thrust fault linkages that exist within a single fold, along with detailed analysis of the spatial extent and form of syn-kinematic packages, provides the basis for a discussion of: (i) the internal structure of a complex fault-related fold, (ii) the geometry and kinematics of thrust fault linkage, (iii) the relationship between folding and faulting in accommodating shortening and (iv) the timing and location of fold growth.

2. Database

This paper is based on a 3D seismic survey (Fig. 2) acquired close to the fold and thrust belt located in the toe-of-slope region of the Niger Delta. The survey covers 2000 km^2, and was acquired with a 6 km offset length, a 12 s record interval and a sampling interval of 4 ms. Inline and crossline spacing is 12.5 m with vertical resolution varying from approximately 7.5 m in shallow levels to 20 m at the base of the thrusted interval. Seismic data were used courtesy of CGGVeritas. Eleven key seismic horizons were mapped in the survey area and dated biostratigraphically by correlation to a nearby confidential exploration well. Interval velocities and check shot data from the well were used to depth convert seismic sections for use in restoration, shortening calculations and to validate geometric structural observations. Seismic lines perpendicular to the regional strike of fold and fault structures were used for fault interpretation, fault heave measurements and calculations of shortening.

3. Structural setting

The seismic survey is located close to a gravity-driven fold and thrust belt in the deepwater Niger Delta (Fig. 3a and b), which has

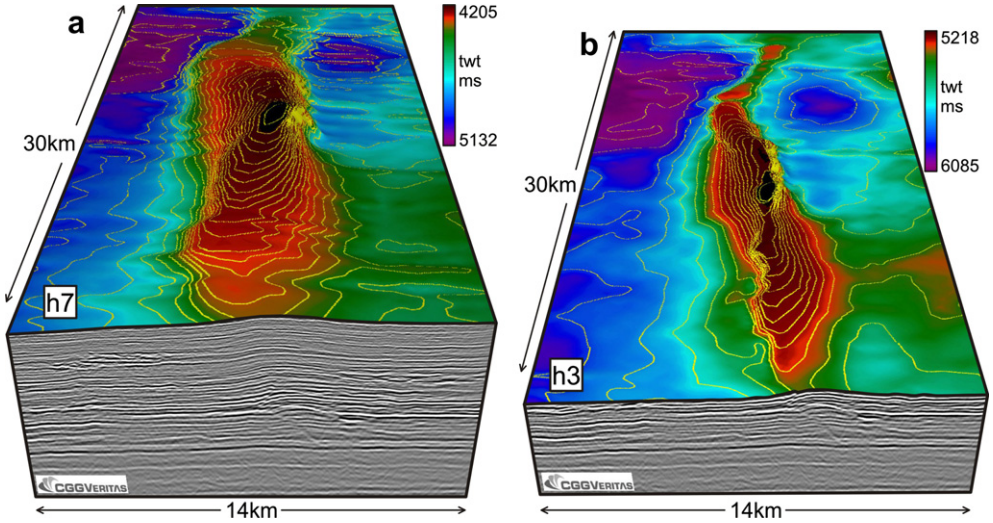

Fig. 2. Part of 3D seismic survey. Two selected stratigraphic horizons (h7 and h3) showing a single, isolated thrust-related fold. Horizon h7 is stratigraphically above horizon h3. Elevation of the horizon is presented in two-way time (ms). Note the change in fold vergence along strike indicated by closely spaced contours (yellow lines). Red/orange colours, structural highs. Purple/blue colours, structural lows. Contour interval: 40 ms. All seismic data are shown courtesy of CGGVeritas.

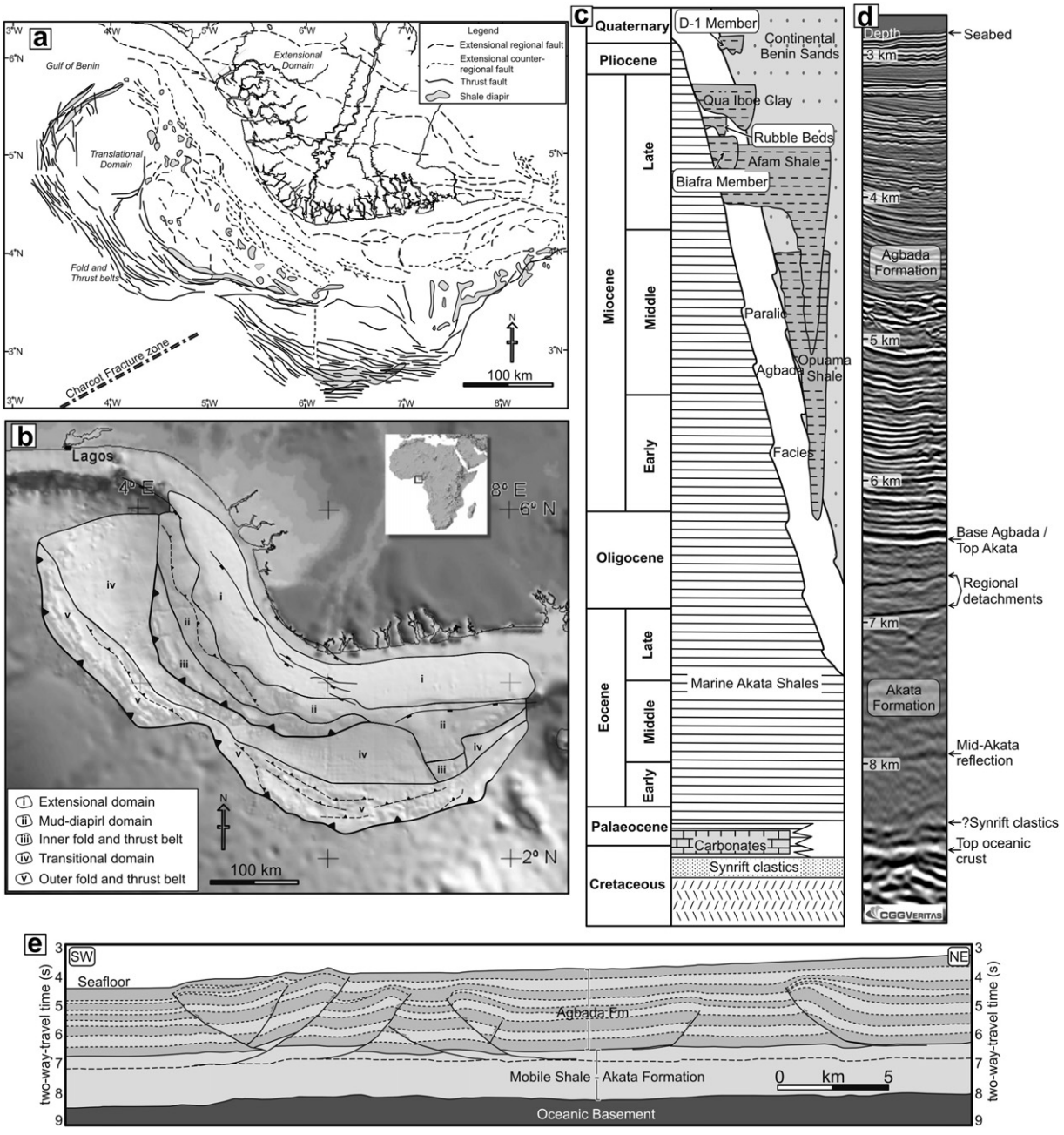

Fig. 3. (a) Regional structural map of extensional, diapiric and contractional features. Locations of shale diapirs taken from Saugy and Eyer (2003). (b) Regional map of the Niger Delta showing the main structural domains. Zones overlay a high-resolution bathymetry image from Corredor et al. (2005). (c) Schematic diagram of the stratigraphic column of the Niger Delta modified after Jubril et al. (1998). (d) Seismic reflection profile to show the seismic facies of the main stratigraphic units in the deep water outer thrust belt. (e) Representative profile through outer fold and thrust belt interpreted from seismic data showing the two main detachment levels for thrusts described in this study.

been the focus of many regional studies (e.g. Short and Stauble, 1967; Onuoha and Ofoegbu, 1988; Doust and Omatsola, 1990; Cohen and McClay, 1996). Deltaic sedimentation began during the late Paleocene to Eocene on the underlying Albian marine succession (Fig. 3c). Neogene clastic sediments are thought to reach a maximum thickness of 12 km in the Niger Delta (Whiteman, 1982). Gravitational collapse of the delta is driven by differential progradational loading and results in the downslope translation of the paralic Agbada Formation (e.g. Bilotti and Shaw, 2005) on major detachment levels that exist within pro-delta marine shales of the Akata Formation (e.g. Briggs et al., 2006) (Fig. 3d). The Niger Delta has three structural zones: an extensional province beneath the outer shelf comprising listric growth faults; a zone of mud diapirism located beneath the upper continental slope; and a more distal contractional zone (Damuth, 1994).

This deep water contractional zone has been subsequently subdivided to differentiate two fold and thrust belts with differing degrees of forethrusts and backthrusts (e.g. Connors et al., 1998; Corredor et al., 2005) (Fig. 3b). The inner thrust belt predominantly has oceanward-verging imbricate thrust faults and folds, and some detachment folds. The outer belt, in contrast, has both landward- and oceanward-verging thrusts and folds (Corredor et al., 2005; Briggs et al., 2006). Separating the two is a transitional detachment-fold zone exhibiting large areas of little or no deformation.

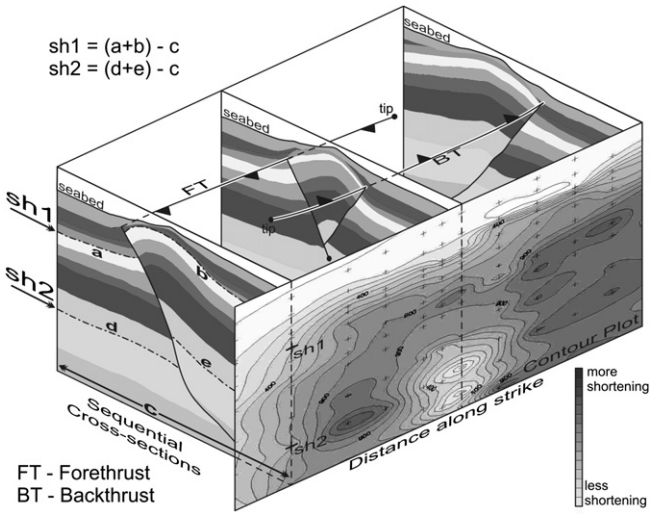

Fig. 4. Methodology for calculating shortening and the display of strike-projected contour plots. Three sequential depth-converted cross-sections showing a change in structural geometry along strike through an antithetic thrust fault linkage. Values of shortening (e.g. sh1, sh2) are calculated by line length analysis. (a, d) Length of selected stratigraphic horizons in the footwall. (b, e) Length of selected horizons in the hangingwall. (c) Length of section. Values of shortening (e.g. sh1, sh2) are plotted on a vertical strike projection plane at depths corresponding to undeformed, 'regional' horizon depths downdip of the fold structures to allow correlation with fault heave measurements. Values are contoured.

The focus of this study is an isolated, fault-related fold located within this transitional detachment fold zone.

Gravitational deformation is active at present, having initiated in the early Tertiary on detachments as a result of overpressure in the shaly Akata unit (Morley and Guerin, 1996; McClay et al., 1998). Thrust faults are documented as detaching at numerous levels within the succession of the Niger Delta (e.g. Corredor et al., 2005; Briggs et al., 2006) although only two detachment levels, at the Agbada–Akata Formation boundary and a regional detachment within the Akata Formation, are seen in these data (Fig. 3e). In this study area, the Agbada Formation comprises a series of compensationally stacked deepwater channel-levee systems (e.g. Deptuck et al., 2003) and is deformed by both oceanward-vergent forethrusts and landward-vergent backthrusts. The relative age of thrust and fold initiation does not simply progress from the foreland into the hinterland. Thrust systems can locally show signs of both break-forward and break-backward thrusting (Corredor et al., 2005).

4. Methods

4.1. Strike-projected contour plots

Shortening values and fault heave measurements are presented using plane-vertical strike projections, following techniques developed for analysis of normal faults (e.g. Rippon, 1985; Walsh and Watterson, 1991). Shortening values are calculated and plotted for eleven seismic marker horizons at a corresponding undeformed, 'regional' horizon depth downdip of the fold structure to avoid introducing spatial positioning errors resulting from variable fold amplitudes (Fig. 4). Fault heave is plotted using the same methodology as for shortening values, rather than at a cut-off position (e.g. Williams and Chapman, 1983) or at the midpoint between cut-offs (e.g. Ellis and Dunlap, 1988). Our plotting convention allows direct comparison between variations in faulting and bulk shortening. The major limitation of our method, however, is that upward displacement gradients along-fault planes cannot be directly compared with previous studies. This restriction will also be true if a fault has a listric character in sectional profile such that a fault decreases in dip with depth, as heave will be seen to increase for the same along-fault displacement. This geometry may produce an apparent increase in the upward displacement gradient. This issue with listric geometry has limited impact however, as faults in this study are approximately planar for the majority of their height as ramps are restricted to within 300–400 ms above the detachment. In addition, the main focus of this paper is on along strike changes in fault and fold geometries, which are unaffected by these limitations.

Shortening values are calculated by simple line length balancing (e.g. Dahlstrom, 1969; Tearpock and Bischke, 1991) (Fig. 4). Fifteen sequential seismic lines spaced along the length of the fold, and perpendicular to the regional fold and fault strike were depth converted using interval velocities from local, unreleased commercial well data. The sections were pinned away from the structure at a point of undeformed layer-cake stratigraphy. The width of the section (c) is subtracted from the summed lengths of the hangingwall (a) and footwall (b) sections of each horizon, such that shortening $(\mathrm{sh}) = (a+b) - c$ (Fig. 4). This method has the advantage of allowing time-efficient calculations that facilitate high-definition plots of the distribution of shortening, and is less prone to errors induced by restoration algorithms and assumptions. Potential error could be introduced due to vertical compaction, an inaccurate velocity model used in depth conversion or pre-thrust ductile thickening. Error analysis involving decompaction and multiple depth conversions suggests these uncertainties fall within acceptable limits (<5% error). It is also argued that these factors may only affect the absolute values for shortening, however this study is more focussed on relative variations in deformation along strike and the expectation is that the limitations of this method are relatively consistent in this direction.

4.2. Timing of deformation

Individual fault-related folds in the deep water Niger Delta are characterised by an upward shallowing of dips above long, planar back limbs suggesting progressive limb rotation during sedimentation (Corredor et al., 2005). The continuity of the majority of syn-kinematic seismic reflections across the fold described in this study indicates sedimentation rates were similar to the rate of structural uplift. Discrete onlap towards the fold crests is rare suggesting that sediment supply generally exceeded fold amplification rate. The onset and duration of folding and faulting are quantified by the analysis of growth packages on the limbs of anticlines (e.g. Medwedeff, 1989; Suppe et al., 1992; Storti and Poblet, 1997). Two variables are defined and measured here; isopach ratios and upward dip reductions.

Isopach ratios compare the depth converted, orthogonal sediment thickness on the fold limbs to those on the crest (Fig. 5) and are expressed as the flank thickness relative to crestal thickness. Assuming the only variation to layer-normal thickness to be due to syn-deformational sedimentation, pre-kinematic sediments should have a constant thickness across a fold, whereas syn-kinematic sediments should thin towards and onto a fold.

Upward dip reductions quantify the change in dip of stratal reflections along vertical profiles positioned on fold limbs (Fig. 5). This reduction is not taken as a direct indication of strain magnitude but instead, as evidence for the location and timing of deformation. Progressive limb rotation due to fold growth causes strata on the flanks to steepen (e.g. Storti and Poblet, 1997), while the depositional surface above them remains subhorizontal. Hence, the dip measured upwards along a vertical profile should show an abrupt decrease as folding begins. Measurements are made on

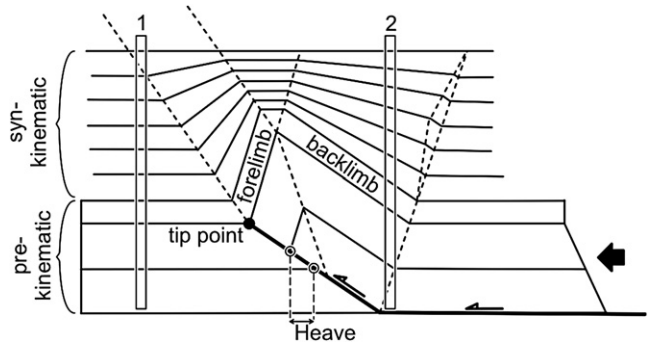

Fig. 5. Diagram of locations of vertical profiles used in calculating isopach ratios and upward dip reductions relative to growth packages associated with the fold. 1, 2: locations of vertical profiles in forelimb and backlimb respectively. Geometry of growth strata adapted from Storti and Poblet (1997) and represents stratal forms associated with fold development predominantly by limb rotation and similar rates of uplift and sedimentation.

depth converted dip-attribute maps that eliminate errors produced by local dip variations such as within channel–levee complexes. Dips of successive horizons are subtracted, and a negative value is interpreted as indicative of a syn-kinematic package. Assuming no internal deformation due to fold-related kinematic behaviour, pre-kinematic sediments, deposited as layer-cake stratigraphy, should have consistent dip along the vertical profile. Comparisons of values recorded by forelimb-backlimb paired profiles provide insights about the degree of fold asymmetry through time (Fig. 5).

5. Results

The case study presented here demonstrates some techniques for strain analysis using 3D seismic data, and provides a basis for the discussion of fault-related fold growth. The anticline consists of numerous faults of opposing dip, and includes synthetic and antithetic fault linkages, along strike fold vergence reversals and irregular fault displacement profiles (Fig. 2). The structure is an isolated fold, located 30 km upslope of the major outer fold and thrust belt, and is fully contained within the seismic survey (Fig. 2). Stratal horizons are offset by a number of forethrusts and backthrusts that detach at, or close to, the Akata-Agbada Formation boundary and link along strike within the fold producing a maximum fold amplitude in excess of 1 km. Surrounding strata are undeformed at a minimum lateral distance of approximately 12 km away from the fold crest.

5.1. Fold shape

Superficially the fold appears to be a simple, single structure (Fig. 2a), however in detail fold and thrust geometries vary along strike and with depth. Changes in fold vergence are interrelated to changes in fault geometry along strike, including the number and dip direction of the faults.

Two key seismic horizons (h7 & h3) mapped in the survey area (Fig. 6) and six representative seismic sections (Fig. 7) are used to illustrate the fold. The fold extends approximately 32 km along strike measured from a reference point at the southern limit of the structure (Fig. 6). Horizon h3 is cut by thrust faults F1, F2, F2b and

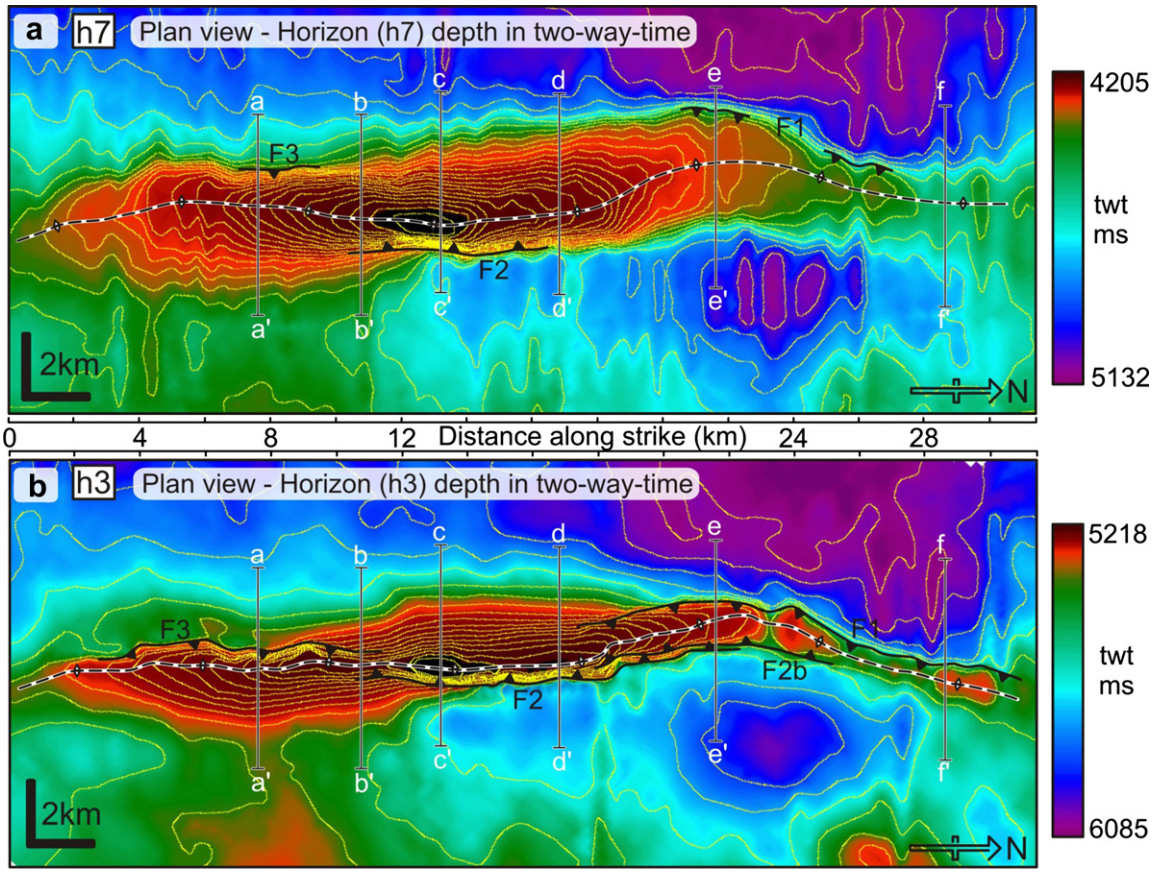

Fig. 6. Maps of horizon elevation in two-way-time (ms). (a) Horizon h7. (b) Horizon h3. Traces of the four major faults are labelled F1, F2, F2b and F3. Fault traces denoted by black triangles in the hangingwalls. Lines a–a′ to f–f′ show locations of the six sections in Fig. 7. Red/orange colours, structural highs. Purple/blue, structural lows. Contour interval: 40 ms.

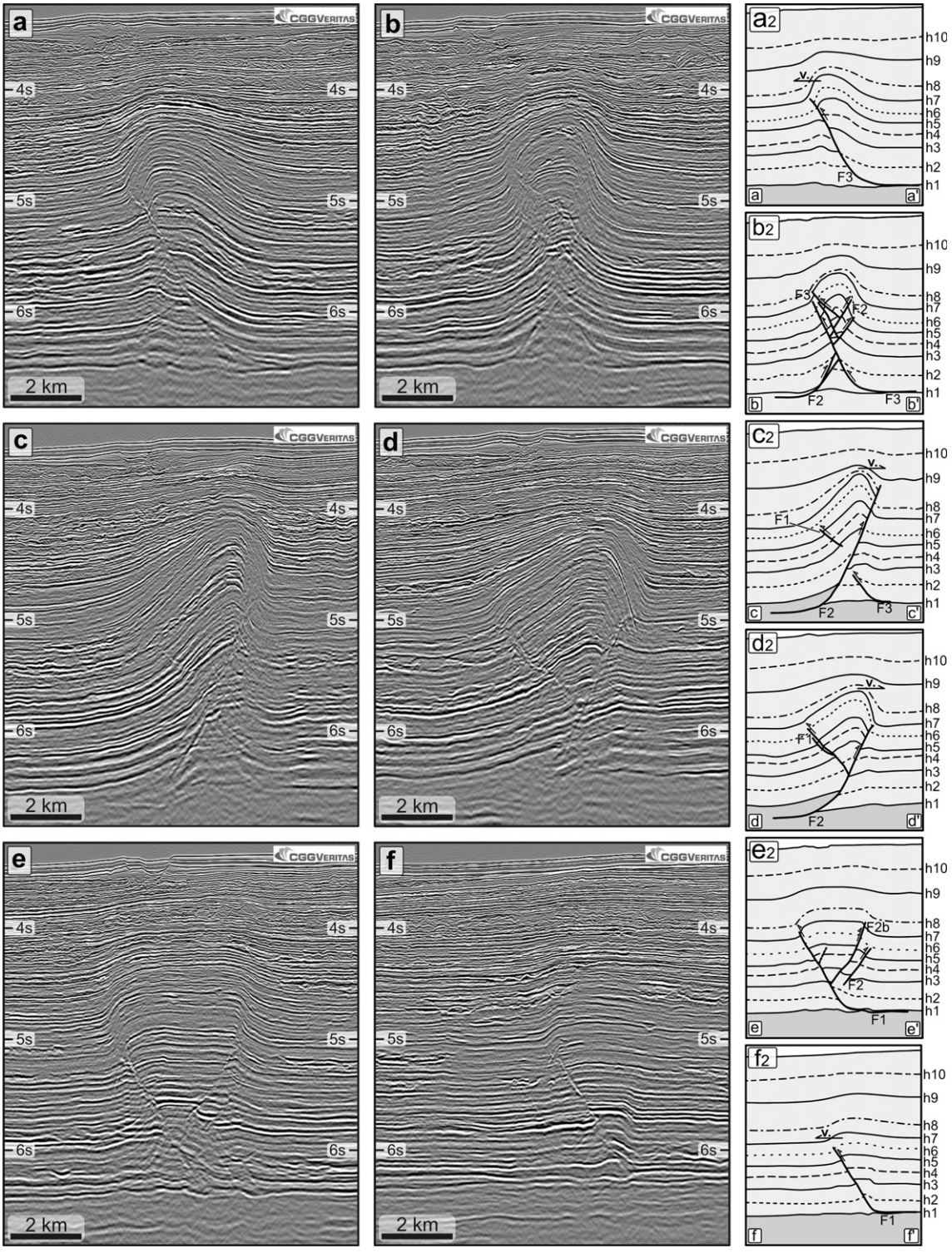

Fig. 7. Selected seismic sections perpendicular to fold trend illustrating changes in fold vergence, fault geometry and fault magnitude along strike. Locations of seismic lines in Fig. 6. All sections are viewed looking north. Sections have an approximate 2.5× vertical exaggeration. Each seismic section (a–f) is displayed along side a seismic interpretation (a2, b2, etc). F1, F2, F2b and F3 are major faults. h1–h10 are regional stratigraphic horizons. v. indicates the direction of vergence of a fold. All seismic data are shown courtesy of CGGVeritas.

F3 along the majority of fold length (from 3 to 31 km along strike) whereas only isolated sections of h7 are offset (Fig. 6). Both horizons exhibit a single structural culmination at approximately 13 km along strike with the fold plunging symmetrically away from this point in both directions. Beyond 26 km along strike the plunge decreases and the fold changes trend by approximately 20°. A local low-amplitude, structural culmination at around 29 km along trend occurs on horizon h3 (Fig. 6b).

The fold vergence varies along strike resulting in an irregular fold shape in plan view, particularly at the level of h3 (Fig. 6b). This horizon has a strong westward vergence at the 8 km mark, but verges eastwards at the culmination at the 13 km position (Fig. 6). The transition

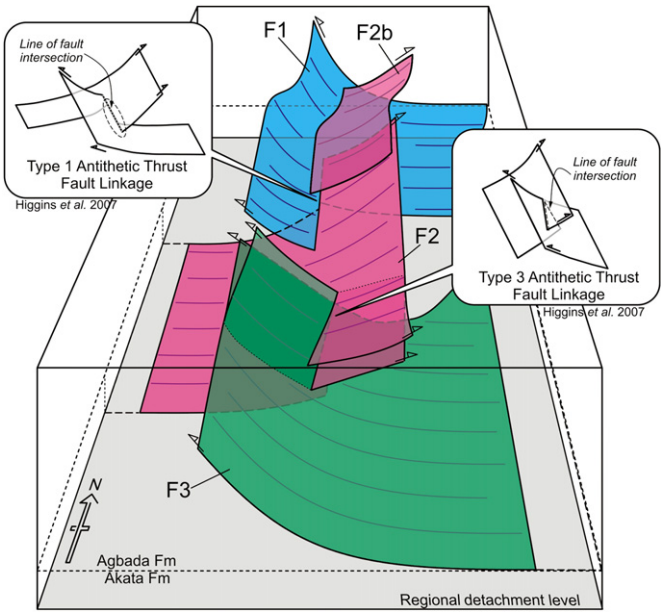

Fig. 8. Three-dimensional conceptual diagram of antithetic fault geometries and linkages. Faults F1 (blue) and F3 (green) detach at the Agbada–Akata Fm boundary. Fault F2 (pink) detaches at a regional level within the Akata Fm (grey surface).

of vergence corresponds to a transfer zone between two major faults, the traces of which can be mapped along the base of the steep limbs. The fold is symmetrical at the centre of these zones. These vergence changes are expressed in hinge deflections on horizon h7 (Fig. 6).

5.2. Internal structure of the fold

The changes in fold vergence along strike with changes in fault geometry (Higgins et al., 2007) are illustrated with representative seismic sections across the fold (Fig. 7). Evidently, fault distribution, orientation and heave magnitude vary significantly along strike. Towards the southern end of the fold, a single forethrust (F3), detaching close to the Agbada–Akata interface (h1), carries a westward verging hangingwall anticline (Fig. 7a). Approximately 5.5 km to the north, the dominant fault is a backthrust (F2) that detaches within the Akata with an eastward-verging hangingwall anticline (Fig. 7c). Two smaller faults, F1 and F3, are imaged in the hangingwall and footwall, respectively. Towards the northern end of the structure, fold amplitude is small, vergence is westward and a small-displacement, single forethrust (F1) is present (Fig. 7f).

The transitions from one fault to another along strike are in the form of antithetic thrust fault linkages (Fig. 7b, d and e, Fig. 8) (Higgins et al., 2007). The backthrust (F2) dominates the central portion of the fold and links with forethrusts F1 to the north and F3 to the south. Higgins et al. (2007) used the vertical extent of a fault relative to branch lines of antithetic faults to describe three types of antithetic fault linkage, two of which occur in the fold featured here (Fig. 8). Faults F1 and F2 interact in a Type 1 linkage (Higgins et al., 2007) as they overlap exclusively above their branch line such that the lateral tip regions are located in the hangingwall of the counterpart fault (Figs. 7d/e and 8). Faults F2 and F3 form a complex cross-cutting relationship within the transfer zone indicative of Type 3 antithetic thrust fault linkages (Higgins et al., 2007) where both faults are present in the footwall and hangingwall of each other (Figs. 7b, 8).

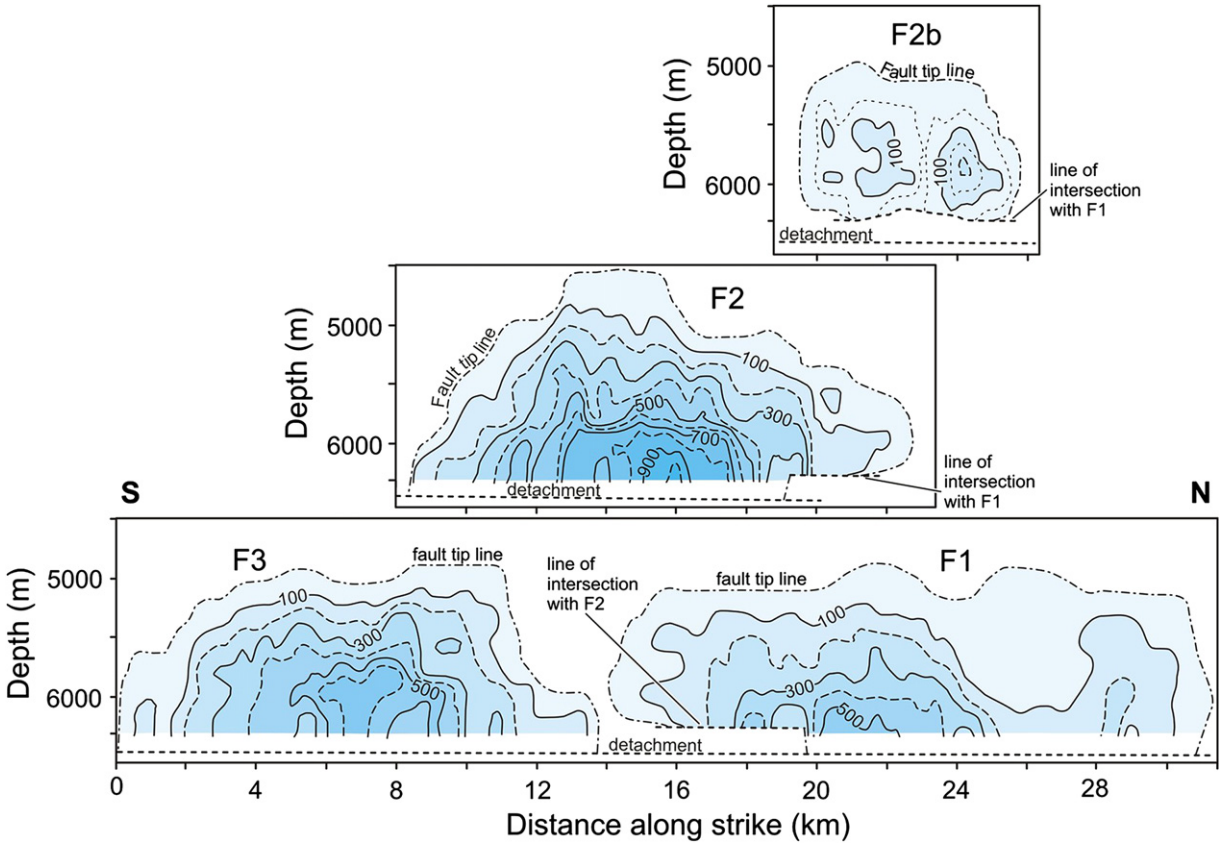

Fig. 9. Fault heave strike-projected contour plots for each major detaching fault (F1, F2, F2b and F3). Contours denote values of fault heave in metres. Zero contour labelled as 'fault tip line'. Data are not projected for horizons immediately above the detachment as measurements are unreliable in the listric zone where faults ramp out of the detachment with significant fault curvature. Branch lines with antithetic faults are indicated by 'lines of intersection'.

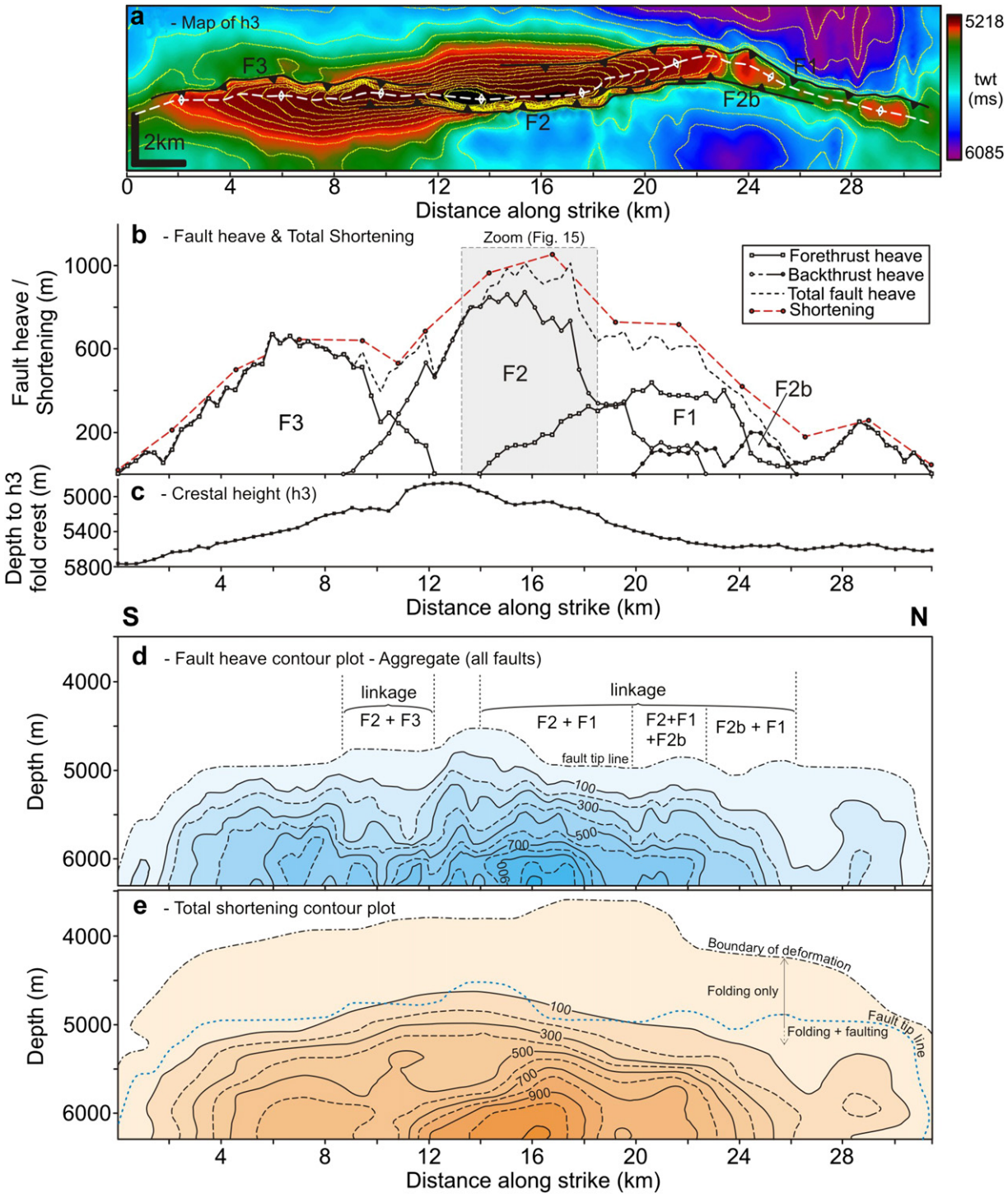

Fig. 10. Aggregate values of fault heave and shortening. (a) Map of h3 horizon in two-way time with fault traces. Fold is aligned with the graphs and contour plots below. Contour interval: 40 ms (b) Heave-distance profiles for each fault. Dashed line. (c) Depth to fold crest for horizon h3. (d) Aggregate fault heave strike-projected contour plot. Lateral overlap of faults F1, F2, F2b and F3 indicated in linkage bracket. (e) Total shortening strike-projected contour plot.

5.3. Individual fault heave profiles

Strike projection heave plots of the four main faults (Fig. 9) commonly have irregular-shaped contours, exhibit several maxima and have lateral tips located some distance above the detachment. For the most part, strike-projections of the detaching thrusts do not resemble an ideal semi-elliptical profile, with the exception of the southern portion of fault F3 (c. 0–5 km along strike) which displays smooth, evenly spaced contours (Fig. 9). The largest deviations in contour patterns occur within the zones of antithetic fault linkage. Lateral tip regions within the F2/F3 linkage, for instance (c. 8–14 km along strike), are downwards-tapering and faults display tip lines that are concave-up in shape (F3).

Fault F3 is the only fault to reach a detachment along its entire length. Faults F1 and F2 interact in a Type 1 antithetic thrust fault linkage (Higgins et al., 2007) such that within the transfer zone,

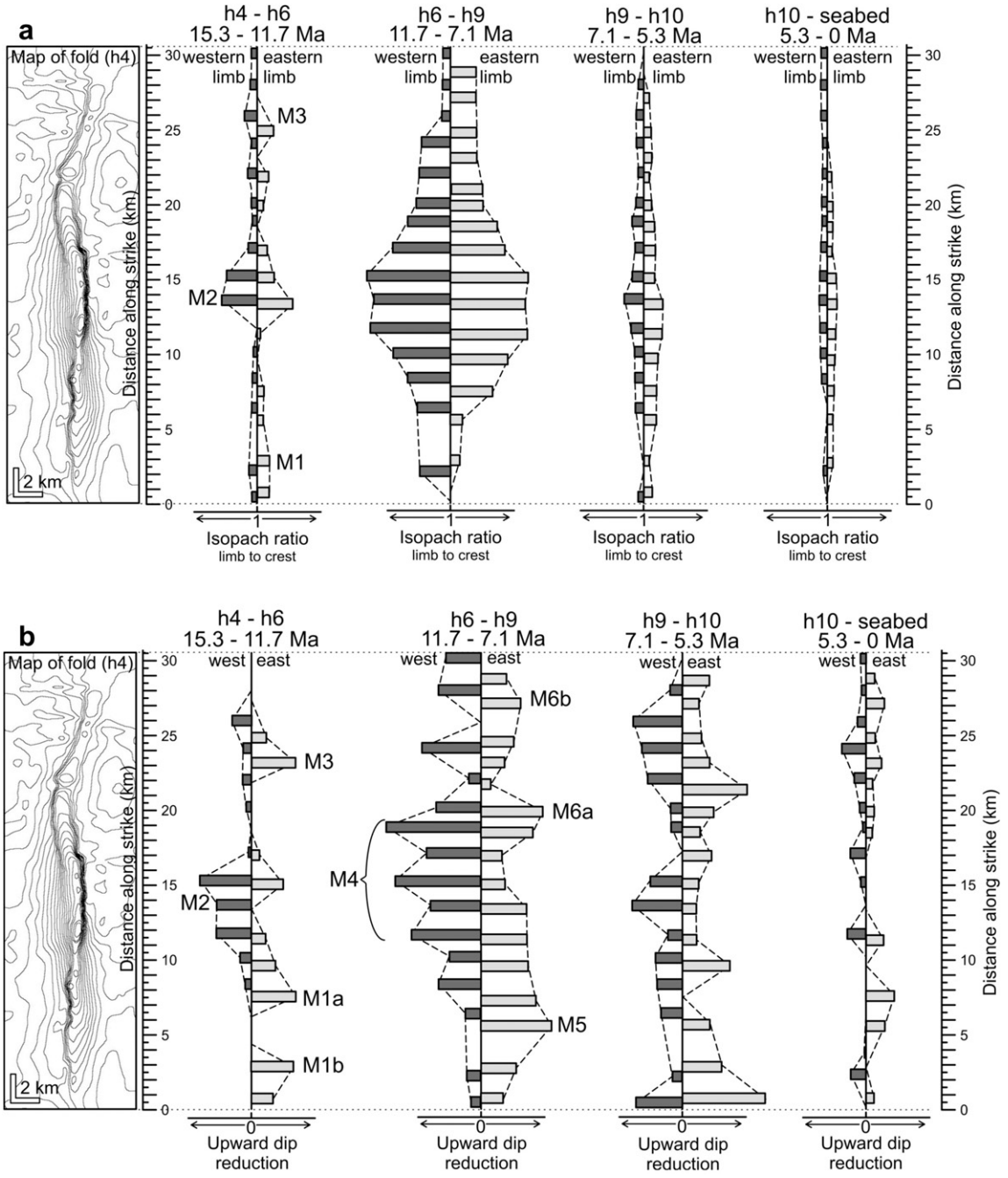

Fig. 11. Analysis of distribution and spatial extent of syn-sedimentary units within the stratigraphic column. (a) Isopach ratios (comparing orthogonal thickness of sediments on the limbs of a fold to those on the crest). Calculated for 17 vertical profiles along length of the fold and displayed as bar charts. Ratio of 1 = no growth. Large bar, large syn-sedimentary fold growth. Small bar, modest syn-sedimentary fold growth. Presented with reference to four time periods, delineated by horizons h4–h6, h6–h9, h9–h10 and h10–seabed. M1, M2 and M3 indicate three areas of large isopach ratio separated by small ratios in the h4–h6 unit. (b) Values for upward reductions in dip. Presentation of results is as in (a). Note asymmetry of the plot due to differing value of upward reductions in dip on each limb. M1a, M1b, M2 and M3 indicate similar areas of early fold growth in the h4–h6 unit as in (a). M4, M5, M6a and M6b indicate areas of growth in the h6–h9 unit.

lower tiplines are not located in the zone of bed-parallel shear within the detachment, but form a branch line with the counterpart fault at around 6300 m depth (Fig. 9). Faults in the northern part of the fold (c. 14–32 km) also have lateral tips that are stratigraphically higher than both the detachment and the branch lines, at between 5750 and 6000 m depth (Fig. 9). At 21 km along strike, for instance, the lower tip line of fault F2 ceases to form a branch line with fault F1 and climbs northwards into hangingwall strata, such that the most lateral part of the fault is located at c. 6000 m depth (Fig. 7e).

The stratigraphic level and relative location of zones of maximum fault heave varies for each fault (Fig. 9). None conform to an ideal central location on, or immediately above, the detachment. The most striking characteristic of fault F1 is the two distinct maxima in fault heave along its length, the first centred at c. 22 km along strike and the second at the 28.5 km position. The minimum that separates the two corresponds to a saddle in the fold on the h3 horizon at around 26 km along strike (Fig. 6b). Fault F3, in contrast, has a single, central maximum (between 6 and 8 km alongstrike)

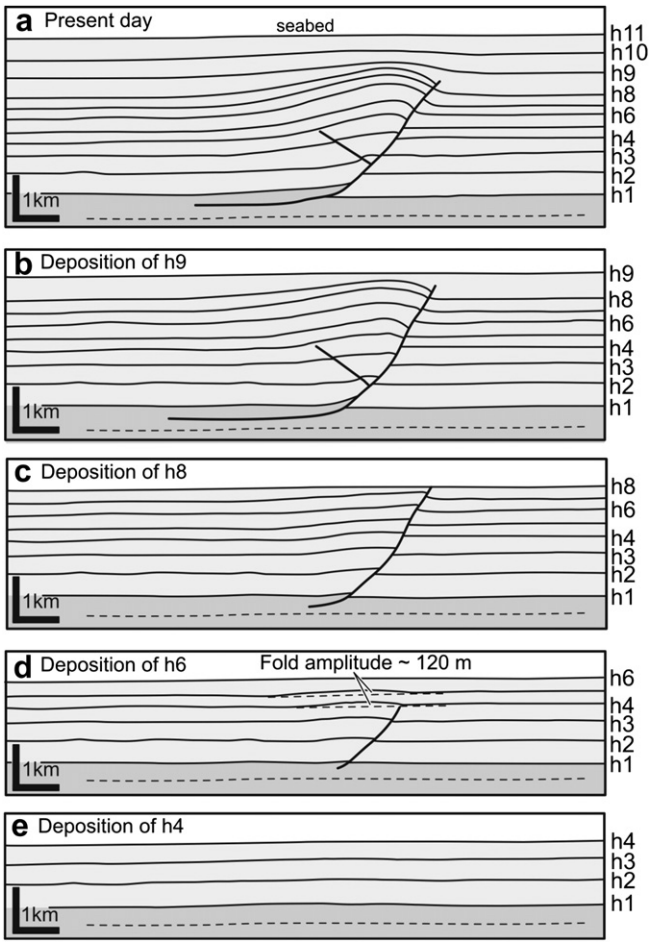

Fig. 12. Sequential restoration of depth-converted seismic profile. Section located between seismic lines c and d (Fig. 7) and viewed looking north. Depth conversion used vertical ray paths and interval velocities obtained from a nearby confidential exploration well. Restoration with 2DMove™ software from Midland Valley Exploration. No vertical exaggeration.

but also displays mushroom-shaped contours, such that sections taken either side of the maxima would record greatest displacement some distance above the detachment, at approximately 5800 m depth. Fault 2 has a central maximum value 16 km along strike, but this position does not correlate with the greatest vertical extent of the fault (13–15 km along strike) due to asymmetry in the lateral extent of the tip line.

5.4. Aggregate heave and shortening profiles

The complexity of the fault heave (Fig. 9) may by analogy with normal faults be largely attributed to displacement transfer onto adjacent structures, interaction with the free surface or changes in the mechanical properties of layered sequences (Barnett et al., 1987; Childs et al., 1993, 2003; Nicol et al., 1996). If modifications to fault profiles are largely due to interaction with neighbouring structures, we might expect to see compensation for displacement deficits in one structure, by enhanced development of neighbouring features, thereby invoking some notional kinematic coherence for the array (Walsh and Watterson, 1991). We now consider fault heave and shortening values for the fold as a whole (Fig. 10) to establish if aggregated faults demonstrate geometric and kinematic coherence.

The northern end of the fold (13–32 km along strike), involving the aggregation of faults F1, F2 and F2b, is characterised by a smooth summed heave-distance profile (Fig. 10b) and aggregate strike-projection (Fig. 10d). This geometry is inferred to be the product of complementary displacement gradients of the constituent faults. This interpretation is exemplified by corresponding, abrupt changes in heave gradient between F2 and F2b at c. 20 km along strike, and between F1 and F2b at c. 24 km along strike (Fig. 10b). Summed fault heave contours better resemble semi-ellipses in this region and there is no evidence of heave deficits due to linkage within the transfer zones (Peacock and Sanderson, 1991; Walsh and Watterson, 1991). The along strike profile of crestal height also shows no evidence for geometric changes related to changes of fault linkage in the northern part of the fold (Fig. 10c).

The southern end of the fold (0–13 km along strike) containing faults F2 and F3 displays a modest deficit in the summed heave-distance profile between c. 9 km and 13 km (Fig. 10b). The aggregate strike projection also shows that the fault tip line and the 100 m heave contour maintain elevation, whereas the 200 and 300 m contours lose elevation within the transfer zone.

The primary heave and shortening maxima are at 16 km within the main fold profile, which is symmetrical in plunge between 0 and 26 km with a culmination at 13 km. However, the fold has a northerly section beyond 26–32 km that correlates with the occurrence of a second, lesser maximum in the fault heave at just over 28 km.

5.5. Isopach ratios

Analysis of isopach ratios of the biostratigraphically defined units h1–h11 suggests the sedimentary sequence can be separated into syn-kinematic and pre-kinematic packages delineated approximately by the h4 horizon. Pre-kinematic sediments within the Agbada Formation, h1–h4, display uniform orthogonal thickness across all parts of the fault and fold. The syn-kinematic package, separated into four units using key seismic horizons, demonstrates systematic variations in the isopach ratios along the fold axis (Fig. 11a).

It is intuitive to expect the along strike trend of the amount of fold growth to resemble that of the amplitude of the fold, as the structure must necessarily have grown most at its culmination. The h6–h9 unit demonstrates just such a relationship (Fig. 11a). The magnitude of fold growth steadily decreases to zero at the tips, away from a maximum located around 12–15 km along strike. Fold growth is largely symmetrical around the central maximum that corresponds to the fold culmination. This relationship is repeated, albeit with smaller isopach ratios, in units h9–h10 and h10–seabed (Fig. 11a). The earliest evidence of growth however, given by the h4–h6 unit, illustrates a different pattern of isopach ratios. Three maxima exist along strike, labelled M1, M2 and M3 (Fig. 11a), separated by areas of little to no fold growth. The maximum isopach ratio (M2) in this time period is recorded approximately 13.5 km along strike. We interpret this geometry of isopach ratios to mean that at the earliest stages of fold conception, the structure was at least three individual folds that amalgamated by the time of h6 deposition into one culmination.

5.6. Upward reduction in dip

Observations of upward reductions in dip complement isopach analysis and give an indication of downdip asymmetry of a fold through time (Fig. 11b). This technique is a valuable addition to the more standard approaches used to assess syn-kinematic packages, and key data can be easily and swiftly extracted from 3D seismic data. Asymmetric folds, such as the example here, will

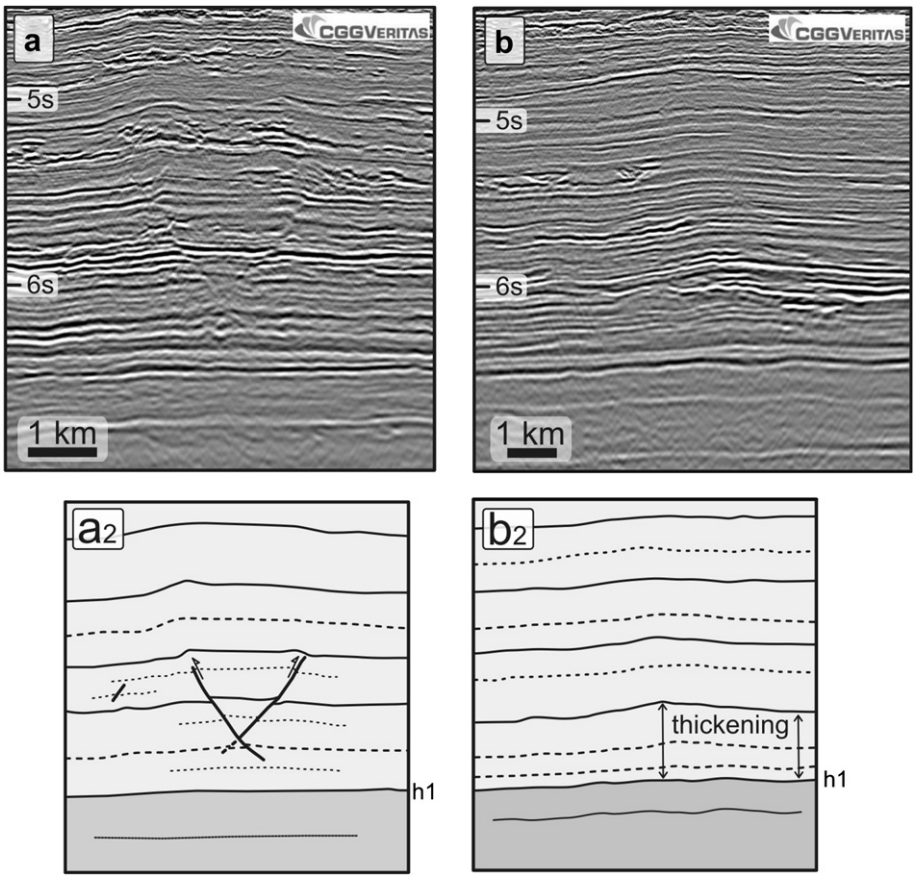

Fig. 13. Two seismic sections showing examples of structures near one end of the fold. (a) Low-amplitude, mildly asymmetric anticline with a forethrust and backthrust of approximately equal displacement. Neither fault reaches the detachment in this section. Maximum displacement on both faults is at about the level of the h3 horizon. (b) Low-amplitude symmetric, unfaulted detachment fold. Interpretations of each section is given in (a2) and (b2). Seismic section (a) is closer to the end of the fold than section (b). All seismic data are shown courtesy of CGGVeritas.

produce consistent differences between data values for the east and west limbs due to unequal limb lengths and dips across the fold. Results suggest that the fold began to grow no earlier than the time of h4 deposition as bounding surfaces are sub-parallel in underlying units. The analysis of upward reductions in dip must be done with depth converted surfaces and horizons, because seismic time sections may not show true growth stratal geometries (Fig. 7).

Important variations are present along strike for each interval. The three most recent time periods (h6–h9, h9–h10 and h10–seabed) all show the fold to be active along its entire length, however the trends in magnitude of the values do not match those of the isopach analysis (Fig. 11b). Several maxima occur in all time periods, as opposed to one central high, and are interpreted as reflecting local, asymmetric fold growth and are coincident with the locations of present-day faults. In unit h6–h9, for example, the western limb is characterised by a broad zone of relatively large upward dip reduction values (labelled M4, Fig. 11b) at the fold centre, between 12 and 18 km along strike. This maximum corresponds to the portion of the present-day fold that has a dominant eastward vergence and incorporates the area of maximum heave of backthrust F2 (Fig. 9). The eastern limb, on the other hand, displays three distinct regions of increased dip reduction values centred at approximately 6, 20 and 28 km along strike, labelled M5, M6a and M6b, respectively (Fig. 11b). M5 corresponds closely with the zone of maximum heave of forethrust F3 at 6–8 km along strike (Fig. 9). M6a and M6b are coincident with the two displacement maxima of forethrust F1, where the first is located between 20 and 22 km and the second at just over 28 km along strike (Fig. 9).

6. Discussion

6.1. Fold growth by segment linkage

Examination of the earliest periods of fold development (Fig. 11) indicates that the featured fold was initially at least three structural culminations separated along strike by saddles or areas of limited fold growth (Fig. 11). The locations of early saddle points are consistent with the sites of present-day transfer zones between the major faults. The positions of the early folds also correspond to regions of present-day strong fold vergence, where one of the three major faults (F1, F2, F3) dominates the accommodation of shortening. Upward dip reduction values also suggest that these early folds quickly developed downdip asymmetry. While the timing of fault initiation cannot be determined conclusively from the data presented, restorations of depth sections are consistent with a thrust initiating with or early in the anticline amplification (Fig. 12). However, although the restoration supports and early thrust initiation, other combinations of assumptions and preferences could allow a restoration with a different early history (e.g. Rowan, 1997). It is beyond the scope of the present work to consider all such possible combinations.

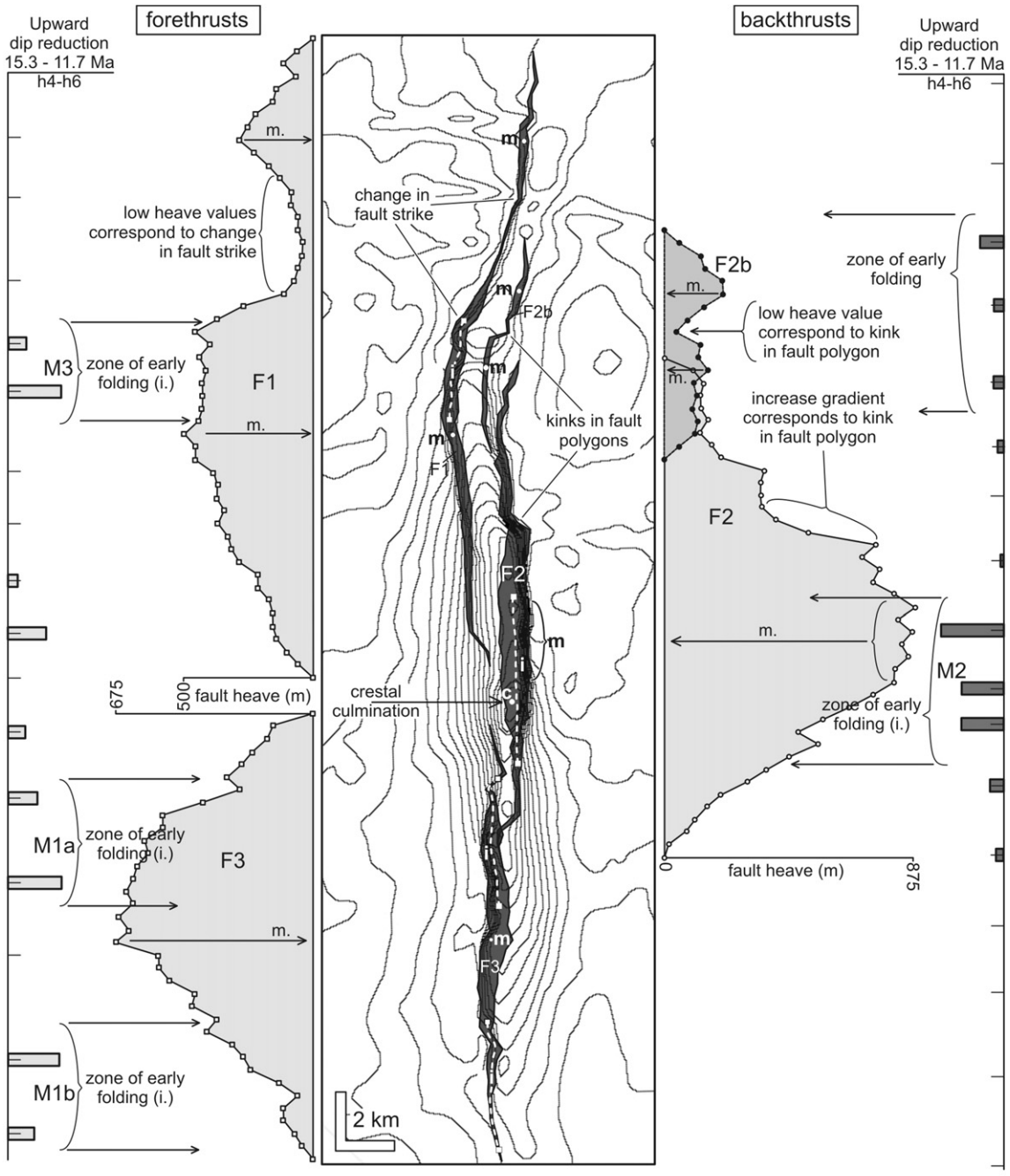

Fig. 14. Correlation of the location of early fold culminations (as indicated by upward dip reductions) with present-day locations of maximum fault heave. Figure also contrasts areas of abrupt gradient change on heave-distance plots (shaded graphs) with changes in trend of fault traces (given by shaded fault polygons on map). Upward dip reductions for h4–h6 time period given as bars. Fault heave-distance profiles (F1, F2, F2b and F3) given as shaded line graphs. m., Point of maximum fault heave along length of fault trace; i., area of early fold growth (dashed white lines); c., location of crestal culmination. Contours on map illustrate topography of horizon h3 (see Fig. 6).

The existing data do not provide a geometric basis, such as pre-tectonic layer deflections, for the locations of the initial fold culmination and thrusts. The generation of numerous faults of opposing dip for this tectonic province of the Niger Delta has previously been explained by the inference of a weak basal detachment, from critical taper wedge modelling (Bilotti and Shaw, 2005). This condition implies the maximum principal compressive stress to be subhorizontal, close to the angle of the decollement, and would suggest that neither forethrusts nor backthrusts have a mechanical advantage with respect to preferential initiation. In such a scenario, the faults of opposing dip would have similar dip angles and be equally efficient at accommodating shortening (Bilotti and Shaw, 2005). If the geometry near the termination of a fold may be used to provide insight into the early deformation history around the fold culmination, then structures near the end of the fold support an initially symmetric deformation geometry (Fig. 13). Both conjugate thrusts in a symmetric anticline (Fig. 13a) and a symmetric anticline without faults (Fig. 13b) occur near a present lateral fold termination.

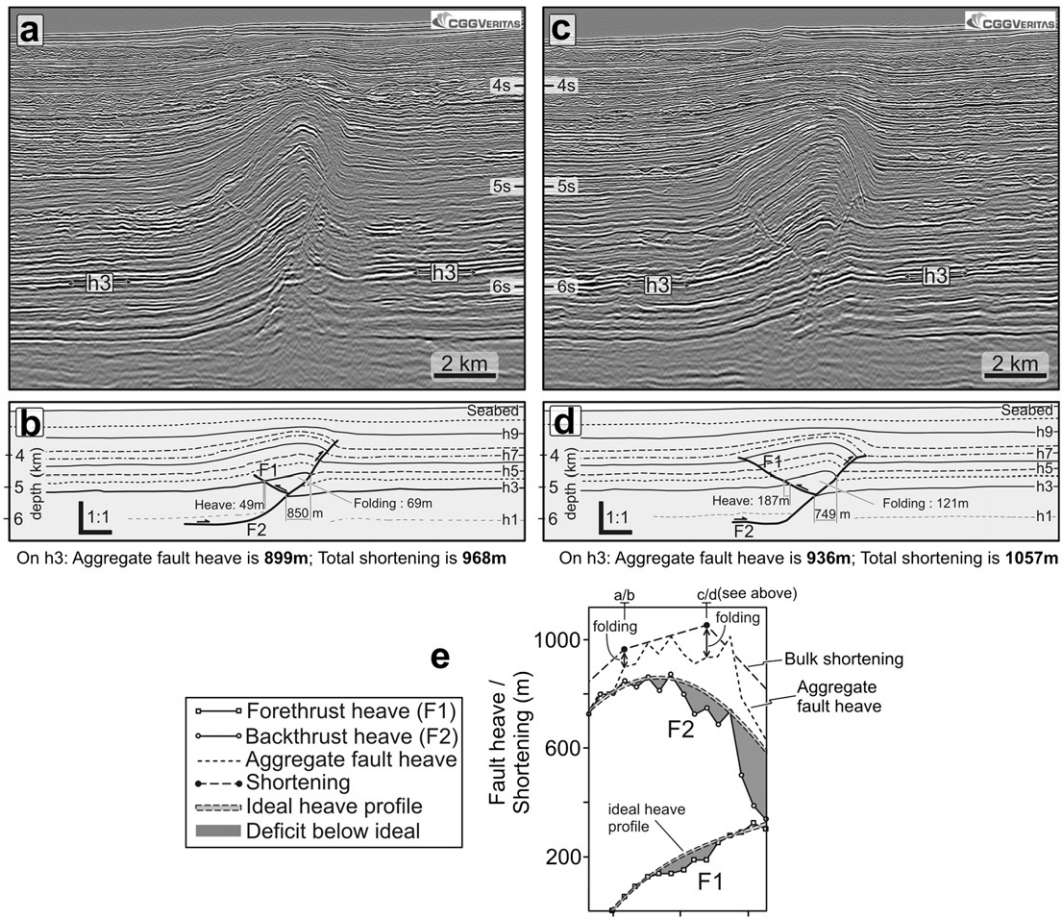

Fig. 15. Comparison of two seismic sections to demonstrate changes in the magnitude of fold-related strain along strike. Analysis of strain made with respect to horizon h3. (a,c) Seismic sections in two-way travel time. h3 Horizon labelled. (b, d) Depth converted cross-sections of (a) and (c) displayed at 1:1. F1, F2 indicate main faults. Values of heave are indicated for the h3 horizon. (e) Enlarged portion of the distance-heave profile of Fig. 10b. Note the difference between aggregate fault heave and bulk shortening varies along strike. Locations of sections (a)–(d) indicated on the graph. All seismic data are shown courtesy of CGGVeritas.

Fault interactions in the fold are not exclusively antithetic. Antithetic linkages are easily identified by the observation of a change in fold vergence, the overlap of fault traces in map view and of faults of opposing dip converging on a point in section. Synthetic linkages are less apparent as originally distinct fault planes may have subsequently joined to produce though-going surfaces (e.g. Cartwright et al., 1995; Childs et al., 1995). Evidence remains however, in the form of abrupt changes in the trend of fault traces indicating a relay breach (e.g. Peacock and Sanderson, 1991; Cartwright et al., 1995; Childs et al., 1995), numerous fault displacement maxima on strike-projections (e.g. Liu and Dixon, 1991) and the spatial distribution of the earliest syn-kinematic sequences around a fold.

In Fig. 14, changes in fault strike coinciding with minima or dramatic changes in fault heave are investigated. Fault F2b is the clearest example of fault heave minima corresponding to a kink in fault strike (Fig. 14). The two positions of maximum displacement are separated by a right-lateral jog in the fault trace where a minima is present and that could indicate relay breach during synthetic fault linkage (e.g. Cartwright and Trudgill, 1994; Childs et al., 1995). This geometry is replicated on fault F1, however the change in fault strike occurs more gradually over a greater distance and is coincident with a wide zone along the fault of minimum heave (Fig. 14).

6.2. Displacement transfer

Bulk shortening contours on strike-projections (Fig. 10e) have orderly patterns and regular spacing. Recent deformation along the length of the fold has been accommodated in a manner similar to that of a single structure, and would therefore imply kinematic interaction and the efficient transfer of displacement between constituent faults, through 'transfer zones' (Dahlstrom, 1970). The criteria for kinematic interaction include complementary modifications to fault displacement patterns (Barnett et al., 1987; Walsh and Watterson, 1991) and the observation of relay structures that indicate displacement transfer (Muraoka and Kamata, 1983; Larsen, 1988; Huggins et al., 1995). Each of the three major faults (F1, F2, F3) show abrupt changes to heave-distance gradients (Figs. 9, 10b) that can define the limits of a relay zone (e.g. Peacock and Sanderson, 1991) and in the trend of fault tip lines away from elliptical profiles in zones of linkage (Fig. 9). Displacement appears to have been transferred smoothly between faults F1 and F2 in the northern half of the fold (Fig. 10a) leading to little evidence of linkage on the aggregate fault heave profile (Fig. 10d). The transfer zone between faults F2 and F3, in contrast, produces an area of fault heave deficit when aggregated. It has been suggested that the nature of displacement distributions in transfer zones may be informative of the original kinematic relationship of the linking faults (e.g. Nicol et al., 2002; Walsh et al., 2003). Faults that have been kinematically linked since inception have a summed displacement profile resembling that of a single, isolated fault, with no deficit in the relay zone (e.g. Nicol et al., 2002; Walsh et al., 2003). Initially isolated faults, which subsequently interact through accidental linkage (e.g. Peacock and Sanderson, 1991; Cartwright et al., 1995; Dawers and Anders, 1995), are thought to maintain distinct displacement maxima on the

adjacent fault segments, separated by a deficit in the relay zone. In contractional settings, where both faults and folds accommodate significant amounts of shortening, albeit to varying degrees, it is imperative to include both continuous and discontinuous deformation when considering this kinematic relationship. The comparison of bulk shortening with aggregate fault heave indicates that the deficit in discontinuous deformation (i.e. faulting) around the transfer zone of fault F2/F3 is compensated for by a rise in continuous displacements (Peacock and Sanderson, 1991; Dawers and Anders, 1995; Nicol et al., 2002; Davis et al., 2005), such as folding, as shown by the increased regularity of shortening contours (Fig. 10e).

The relative amount of shortening accommodated by faulting and folding varies in each fault interaction and may be dependent on the mode of antithetic fault linkage. The lesser length of fault overlap in the F2/F3 example, the steeper gradients of heave profiles and the heave deficit within the transfer zone all suggest a greater retardation of lateral propagation rates during linkage (e.g. Peacock and Sanderson, 1991; Nicol et al., 1996) than that in the F1/F2 linkage, resulting in increased fold strain.

6.3. Fault related folding

The relative importance of faulting and folding in accommodating shortening was documented as varying through time during centrifuge modeling of a fold and thrust belt (Liu and Dixon, 1991). Displacement was transferred between folds and faults in time, spatially along strike and between en-echelon fault pairs within transfer zones. Other studies have shown that, in contrast to some established models of fault-related folding in which fault slip accumulation (e.g. Suppe and Medwedeff, 1990) or displacement gradients (e.g. Wickham, 1995) directly relate to fold size, displacement deficits within transfer zones are compensated for by an increase in fold strain (Nicol et al., 2002; Davis et al., 2005). A similar result is recorded in this study as bulk-shortening strike-projections display more regular contour patterns than that of aggregated fault heave (Figs. 5 and 10). This relationship suggests that variation in the amount of folding along strike compensates for fluctuations in the magnitude of fault heave. To test this, two seismic sections across the fold are compared (Fig. 15) with reference to measurements made on the h3 horizon.

Both seismic lines are taken from the southern end of the F1/F2 linkage zone. An enlarged portion of the heave-distance profile of all the faults (Fig. 10b) is included in Fig. 15e to highlight the areas where perturbations in fault heave result in small deficits below idealised fault profiles. The aggregate value of fault heave is similar in each section although the amount of heave accommodated by each component fault varies. The first seismic section (Fig. 15a and b) is located close to the lateral tip of fault F1 and values of heave for both faults plot close to the ideal heave profiles (Fig. 15e). The second section (Fig. 15c and d) is located approximately 2.4 km along strike to the north. Here faults display a cumulative heave deficit of around 10% below the predicted ideal value (Fig. 15e). Folding compensates, to some extent, for the minor variations in fault heave along strike such that measurements of shortening produce a smoother, more elliptical profile. In this example the amount of shortening accommodated by folding almost doubles between the two sections, from 69 m (Fig. 15b) to 121 m (Fig. 15d). It is important to note however that faulting remains the most dominant and important mode of strain accommodation in both cases (see figure for ratios).

7. Summary and conclusions

Strike-projected contour plots for fault heave and bulk shortening values along a single fold in a deep water fold and thrust belt, Niger Delta, are published for the first time. Measurements of growth sequences and detailed fault-plane geometries from 3D seismic data illustrate numerous faults of similar and opposing dip linking along strike in the fold. The data and analyses support the following conclusions:

1. The distribution of bulk shortening along a single thrust fault or numerous linked thrusts is simple, systematic and similar to that observed for extensional faults.
2. Individual heave profiles of overlapping, linked faults show that component faults were kinematically linked throughout development.
3. Deficits in fault heave on non-linking or aggregated profiles and displacement minima within transfer zones are compensated to some degree by an increase in the amount of fold strain. Fold amplitude and fold crest elevation is largely unaffected by minor variations in fault heave.
4. The geometry of growth strata indicates that the evolution of the fold involved the nucleation and along strike amalgamation of three smaller initial anticlines, and at least five thrusts, to create a single fault-related fold with a single culmination.

Acknowledgements

This study forms part of a PhD funded by Statoil at the 3DLab, Cardiff University. We are grateful to CGGVeritas for the release of seismic data. This document was greatly improved by comments from Paul Brockbank and Catherine Baudon, and by the reviews of Brent A. Couzens-Schultz, John Walsh and William Dunne.

References

Barnett, J.A.M., Mortimer, J., Rippon, J.H., Walsh, J.J., Watterson, J., 1987. Displacement geometry in the volume containing a single normal fault. AAPG Bulletin 71, 925–937.
Bilotti, F., Shaw, J., 2005. Deep-water Niger Delta fold and thrust belt modeled as a critical-taper wedge: the influence of elevated basal fluid pressure on structural styles. AAPG Bulletin 89, 1475–1491.
Boyer, S., Elliot, D., 1982. Thrust systems. AAPG Bulletin 66, 1196–1230.
Briggs, S.E., Davies, R.J., Cartwright, J.A., Morgan, R., 2006. Multiple detachment levels and their control on fold styles in the compressional domain of the deepwater west Niger Delta. Basin Research 18, 435–450.
Butler, R.W.H., 1992. Structural evolution of the western Chartreuse fold and thrust system, NW French Subalpine Chains. In: McClay, K.R. (Ed.), Thrust Tectonics. Chapman and Hall, New York, pp. 287–297.
Cartwright, J., Trudgill, B., Mansfield, C., 1995. Fault growth by segment linkage: an explanation for scatter in maximum displacement and trace length data from the Canyonlands Grabens of SE Utah. Journal of Structural Geology 17, 1319–1326.
Cartwright, J.A., Trudgill, B., 1994. Relay-ramp forms and normal-fault linkages, Canyonlands National Park, Utah. Geological Society of America Bulletin 106, 1143–1157.
Childs, C., Easton, S.J., Vendeville, B.C., Jackson, M.P.A., Lin, S.T., Walsh, J.J., Watterson, J., 1993. Kinematic analysis of faults in a physical model of growth faulting above a viscous salt analogue. Tectonophysics 228, 313–329.
Childs, C., Watterson, J., Walsh, J.J., 1995. Fault overlap zones within developing normal fault systems. Journal of the Geological Society, London 152, 535–549.
Childs, C., Nicol, A., Walsh, J.J., Watterson, J., 2003. The growth and propagation of synsedimentary faults. Journal of Structural Geology 25, 633–648.
Cohen, H., McClay, K., 1996. Sedimentation and shale tectonics of the northwestern Niger Delta front. Basin Research 13, 313–328.
Connors, C.D., Denson, D.B., Kristiansen, G., Angstadt, D.M., 1998. Compressive anticlines of the mid-outer slope, central Niger Delta (abs). AAPG Bulletin 82, 1903.
Corredor, F., Shaw, J., Bilotti, F., 2005. Structural styles in the deep-water fold and thrust belts of the Niger Delta. AAPG Bulletin 89, 753–780.
Dahlstrom, C.D.A., 1969. Balanced cross sections. Canadian Journal of Earth Sciences 6, 743–757.
Dahlstrom, C.D.A., 1970. Structural Geology in the eastern margin of the Canadian rocky mountains. Bulletin of Canadian Petroleum Geology 18, 332–406.
Damuth, J., 1994. Neogene gravity tectonics and depositional processes on the deep Niger Delta continental margin. Marine and Petroleum Geology 11, 320–346.
Davis, K., Burbank, D.W., Fisher, D., Wallace, S., Nobes, D., 2005. Thrust-fault growth and segment linkage in the active Ostler fault zone, New Zealand. Journal of Structural Geology 27, 1528–1546.

Dawers, N., Anders, M., 1995. Displacement-length scaling and fault linkage. Journal of Structural Geology 17, 607–614.
Deptuck, M., Steffens, G., Barton, M., Pirmez, P., 2003. Architecture and evolution of upper fan channel-belts on the Niger Delta slope and in the Arabian Sea. Marine and Petroleum Geology 20, 649–676.
Doust, H., Omatsola, E., 1990. Niger delta. In: Edwards, J., Santagrossi, P. (Eds.), Divergent/Passive Margin Basins. AAPG Memoir 48, 201–238.
Elliot, D., 1976. The energy balance and deformation mechanisms of thrust sheets. Philosophical Transactions of Royal Society of London A 283, 289–312.
Ellis, M., Dunlap, W., 1988. Displacement variation along thrust faults: implications for the development of large faults. Journal of Structural Geology 10, 183–192.
Higgins, S., Davies, R.J., Clarke, B., 2007. Antithetic fault linkages in a deep water fold and thrust belt. Journal of Structural Geology 29, 1900–1914.
Huggins, P., Watterson, J., Walsh, J.J., Childs, C., 1995. Relay zone geometry and displacement transfer between normal faults recorded in coal-mine plans. Journal of Structural Geology 17, 1741–1755.
Jamison, W.R., 1987. Geometric analysis of fold development in overthrust terranes. Journal of Structural Geology 9, 207–219.
Jubril, M.A., Shaw, H.F., Fallick, A.E., 1998. Stable isotope and geochemical evidence of formation pore fluid evolution during diagenesis of Tertiary sandstones and mudrocks of the Niger Delta. Journal of African Earth Sciences 27, 417–435.
Larsen, P.H., 1988. Relay structures in the lower Permian basement-involved extension system, East Greenland. Journal of Structural Geology 10, 3–8.
Liu, S., Dixon, D., 1991. Centrifuge modelling of thrust faulting: structural variation along strike in fold-thrust belts. Tectonophysics 188, 39–62.
McClay, K., Dooley, T., Lewis, G., 1998. Analog modeling of progradational delta systems. Geology 26, 771–774.
Medwedeff, D.A., 1989. Growth fault-bend folding at southeast Lost Hills, San Joaquin Valley, California. AAPG Bulletin 73, 54–67.
Meyer, V., Nicol, A., Childs, C., Walsh, J.J., Watterson, J., 2002. Progressive localisation of strain during the evolution of a normal fault population. Journal of Structural Geology 24, 1215–1231.
Mitchell, M.M., Woodward, N.B., 1988. Kink detachment fold in the southwest Montana fold and thrust belt. Geology 16, 162–165.
Morley, C., Guerin, G., 1996. Comparison of gravity-driven deformation styles and behaviour associated with mobile shales and salt. Tectonics 15, 1154–1170.
Muraoka, H., Kamata, H., 1983. Displacement distribution along minor fault traces. Journal of Structural Geology 5, 483–495.
Nicol, A., Walsh, J.J., Watterson, J., Bretan, P.G., 1995. Three-dimensional geometry and growth of conjugate normal faults. Journal of Structural Geology 17, 847–862.
Nicol, A., Watterson, J., Walsh, J.J., Childs, C., 1996. The shapes, major axis orientations and displacement patterns of fault surfaces. Journal of Structural Geology 18, 235–248.
Nicol, A., Gillespie, P., Childs, C., Walsh, J., 2002. Relay zones between mesoscopic thrust faults in layered sedimentary sequences. Journal of Structural Geology 24, 709–727.
Onuoha, K., Ofoegbu, C., 1988. Subsidence and evolution of Nigeria's continental margin: implications of data from Afowo-1 well. Marine and Petroleum Geology 5, 175–181.
Peacock, D.C.P., Sanderson, D.J., 1991. Displacements, segment linkage and relay ramps in normal fault zones. Journal of Structural Geology 13, 721–733.
Rich, J.L., 1934. Mechanics of low-angle overthrust faulting as illustrated by Cumberland thrust block, Virginia, Kentucky, and Tennessee. Bulletin of the American Association of Petroleum Geologists 18, 1584–1596.
Rippon, J.H., 1985. Contoured patterns of the throw and hade of normal faults in the coal measures (Westphalian) of north-east Derbyshire. Proceedings of the Yorkshire Geological Society 45, 147–161.
Rowan, M.G., 1997. Three-dimensional geometry and evolution of a segmented detachment fold, Mississippi Fan foldbelt, Gulf of Mexico. Journal of Structural Geology 19, 463–480.
Saugy, E., Eyer, A., 2003. Fifty years of exploration in the Niger Delta (west Africa). In: Halbouty, M.T. (Ed.), Giant Oil and Gas Fields of the Decade 1990–1999. American Association of Petroleum Geologists Memoir 78, 211–226.
Segall, P., Pollard, D.D., 1980. Mechanics of discontinuous faults. Journal of Geophysical Research B 85, 4337–4350.
Short, K., Stauble, A., 1967. Outline of geology of Niger Delta. AAPG Bulletin 51, 761–779.
Storti, F., Poblet, J., 1997. Growth stratal architectures associated to decollement folds and fault-propagation folds; inferences on fold kinematics. In: Cloetingh, S., Fernandez, M., Munoz, J.A., Sassi, W., Horvath, F. (Eds.), Structural Controls on Sedimentary Basin Formation. Tectonophysics 282, 1–4. Elsevier, Amsterdam, Netherlands, 353–373.
Suppe, J., 1983. Geometry and kinematics of fault-bend folding. American Journal of Science 283, 684–721.
Suppe, J., 1985. Principles of Structural Geology. Prentice Hall, Englewood Cliffs, New Jersey.
Suppe, J., Medwedeff, D.A., 1990. Geometry and kinematics of fault-propagation folding. Eclogae Geologicae Helvetiae 83, 409–454.
Suppe, J., Chou, G.T., Hook, S.C., 1992. Rates of folding and faulting determined from growth strata. In: McClay, K.R. (Ed.), Thrust Tectonics. Chapman and Hall, London, pp. 105–121.
Tearpock, D., Bischke, R.E., 1991. Applied Subsurface Geological Mapping. Prentice Hall PTR, New Jersey.
Thorbjornsen, K.L., Dunne, W.M., 1997. Origin of a thrust-related fold: geometric vs kinematic tests. Journal of Structural Geology 19, 303–319.
Walsh, J.J., Watterson, J., 1991. Geometric and kinematic coherence and scale effects in normal fault systems. In: Roberts, A.M., Yielding, G., Freeman, B. (Eds.), The Geometry of Normal Faults. Geological Society Special Publication 56, pp. 193–203.
Walsh, J.J., Bailey, W.R., Childs, C., Nicol, A., Bonson, C.G., 2003. Formation of segmented normal faults: a 3-D perspective. Journal of Structural Geology 25, 1251–1262.
Whiteman, A.J., 1982. Nigeria; Its Petroleum Geology, Resources and Potential. Grahan and Trotman, London.
Wickham, J., 1995. Fault displacement-gradient folds and the structure at Lost Hills, California (U.S.A). Journal of Structural Geology 17, 1293–1302.
Williams, G., Chapman, T., 1983. Strains developed in the hangingwalls of thrusts due to their slip/propagation rate: a dislocation model. Journal of Structural Geology 5, 563–571.
Woodward, N.B., 1992. Deformation styles and geometric evolution of some Idaho–Wyoming thrust belt structures. In: Mitra, S., Fisher, G. (Eds.), Structural Geology of Fold and Thrust Belts 5. The John Hopkins Studies in Earth and Space Sciences.